AGU PUBLICATIONS

Journal of Advances in Modeling Earth Systems

RESEARCH ARTICLE
10.1002/2017MS001234

Application and Evaluation of an Explicit Prognostic Cloud-Cover Scheme in GRAPES Global Forecast System

Zhanshan Ma[1,2,3], Qijun Liu[2,3], Chuanfeng Zhao[1,4], Xueshun Shen[2,3], Yuan Wang[4,5], Jonathan H. Jiang[5], Zhe Li[2,3], and Yuk Yung[4]

[1]State Key Laboratory of Earth Surface Processes and Resource Ecology, and College of Global Change and Earth System Science, and Joint Center for Global Change Studies, Beijing Normal University, Beijing, China, [2]National Meteorological Center, Beijing, China, [3]Numerical Weather Prediction Center of China Meteorological Administration, Beijing, China, [4]Division of Geological and Planetary Sciences, California Institute of Technology, Pasadena, CA, USA, [5]Jet Propulsion Laboratory, California Institute of Technology, Pasadena, CA, USA

Abstract An explicit prognostic cloud-cover scheme (PROGCS) is implemented into the Global/Regional Assimilation and Prediction System (GRAPES) for global middle-range numerical weather predication system (GRAPES_GFS) to improve the model performance in simulating cloud cover and radiation. Unlike the previous diagnostic cloud-cover scheme (DIAGCS), PROGCS considers the formation and dissipation of cloud cover by physically connecting it to the cumulus convection and large-scale stratiform condensation processes. Our simulation results show that clouds in mid-high latitudes arise mainly from large-scale stratiform condensation processes, while cumulus convection and large-scale condensation processes jointly determine cloud cover in low latitudes. Compared with DIAGCS, PROGCS captures more consistent vertical distributions of cloud cover with the observations from Atmospheric Radiation Measurements (ARM) program at the Southern Great Plains (SGP) site and simulates more realistic diurnal cycle of marine stratocumulus with the ERA-Interim reanalysis data. The low, high, and total cloud covers that are determined via PROGCS appear to be more realistic than those simulated via DIAGCS when both are compared with satellite retrievals though the former maintains slight negative biases. In addition, the simulations of outgoing longwave radiation (OLR) at the top of the atmosphere (TOA) from PROGCS runs have been considerably improved as well, resulting in less biases in radiative heating rates at heights below 850 hPa and above 400 hPa of GRAPES_GFS. Our results indicate that a prognostic method of cloud-cover calculation has significant advantage over the conventional diagnostic one, and it should be adopted in both weather and climate simulation and forecast.

Key Points:
- A prognostic cloud-cover scheme has been implemented into the GRAPES global forecast system to replace the original diagnostic scheme
- The prognostic scheme significantly improved the simulations of cloud fraction vertical structure, including total, low, and high clouds
- The SW and LW radiation at TOA have been better simulated with the prognostic scheme, along with the profiles of radiative heating rate

Correspondence to:
C. Zhao,
czhao@bnu.edu.cn;
Q. Liu,
liuqj@cma.gov.cn

Citation:
Ma, Z., Liu, Q., Zhao, C., Shen, X., Wang, Y., Jiang, J. H., et al. (2018). Application and evaluation of an explicit prognostic cloud-cover scheme in GRAPES global forecast system. *Journal of Advances in Modeling Earth Systems*, *10*, 652–667. https://doi.org/10.1002/2017MS001234

Received 17 NOV 2017
Accepted 17 FEB 2018
Accepted article online 21 FEB 2018
Published online 8 MAR 2018

1. Introduction

It is well known that clouds, which cover about 60%–70% of the globe, play a critical role in weather and climate system (Cantrell & Heymsfield, 2005; Cotton & Anthes, 1989; IPCC, 2013; Liou, 1992; Liou & Ou, 1989). However, it is still challenging to accurately simulate the distributions and evolution of clouds. At present, clouds are one of the largest sources of uncertainty in numerical weather and climate model simulations (Soden & Held, 2006; IPCC, 2013; Jiang et al., 2012; Klein & Jakob, 1999; Stocker et al., 2013; Wang et al., 2013).

Cloud cover is an important cloud physical variable and significantly influences the radiation budget of earth-atmosphere system by modifying both longwave (LW) and shortwave (SW) radiative transfer (Rybka & Tost, 2014; Wang & Zhao, 2017). For instance, a mere 4% increase in the area of the global covered by low level stratus clouds would be sufficient to offset the 2–3 K predicted rise in global average temperature due to a doubling of CO_2 (Randall et al., 1984). Obviously, it is crucial that numerical climate and weather prediction models resolve realistic cloud cover as accurate as possible. Determination of the cloud cover in large-scale models is difficult because the air motion and cloud particles occur on time and space scales far smaller than typical resolution of model grid box. Consequently, cloud cover is generally parameterized in terms of the large-scale variables. One key problem in the representation of cloud cover in large-scale models is how to estimate cloud cover in a partially cloudy grid box (Teixeira, 2001). To improve simulation of horizontal cloud cover, great efforts have been undertaken to develop more reliable cloud-cover schemes in the past few decades. The various cloud-cover schemes can be divided into the following three major types: statistical, diagnostic and prognostic approaches (Akihiko et al., 2008; Dai et al., 2004).

Statistical approaches are based on the idea that clouds could occur on a subgrid scale when the humidity and its saturation values are somehow distributed around their grid-mean value. Most statistical cloud-cover schemes specify the underlying distribution of humidity and temperature variability at each grid box, determine a suitable form for the probability distribution function (PDF) of total water fluctuations, and then derive a definition about the higher order moments of the distributions. Nevertheless, it is very hard to theoretically derive a PDF form for statistical schemes. Currently, the adopted distributions for instance Gauss, lognormal, and exponential are all unbounded functions, which make the maximum cloud condensate mixing ratio approach infinity, and part of the grid cell is always covered by clouds (Tompkins, 2005). Of course, there are truncated Gaussian and Gamma functions that can be used (Huang et al., 2014; Tompkins, 2002).

Diagnostic schemes parameterize cloud cover by simply specifying a function for the relationship between cloud cover and grid-averaged variables such as relative humidity (RH; Slingo, 1987; Sundqvist et al., 1989) or cloud water contents (Dowling & Radke, 1990) or both RH and cloud water contents (Xu & Randall, 1996). Because the diagnostic schemes can successfully capture the basic characteristics of cloud cover and are simple, they are widely used in large-scale models (Slingo, 1987). However, the diagnostic schemes are short of firm physical basis (Wetzel & Bates, 1995) and cannot represent the interaction between clouds and atmospheric processes related to hydrological cycle in large-scale models. For example, diagnostic scheme is difficult to reproduce the long-lasting anvil cloud cover in connection with cumulus convection processes and fails with respect to the simulations of tropical and subtropical clouds (Randall, 1989; Randall et al., 1989). Teixeira (2001) argued that a coupling with the convection parameterization in the cloud-cover scheme is important in order to obtain a realistic distribution of clouds.

The prognostic approaches could overcome the deficiencies mentioned above. For this type scheme, cloud cover is simulated as a prediction variable using an equation composed of source and sink terms of clouds (Tiedtke, 1993; Wilson et al, 2008a, 2008b). The source and sink terms are commonly connected with subgrid-scale processes such as cumulus convection, planetary boundary layer turbulence, and the large-scale stratiform condensation and evaporation processes. The prognostic cloud-cover scheme was first proposed by Tiedtke (1993), followed by other prognostic schemes. These prognostic schemes have been implemented into a number of large-scale models (Jakob, 1999; Park et al, 2016; Wang, 1996; Wilson et al., 2008a). For example, Tiedtke's prognostic scheme was used in the European Center for Medium-Range Weather Forecast (ECMWF) Integrated Forecast System (IFS) and the Geophysical Fluid Dynamics Laboratory (GFDL) Global Atmosphere Model version2 and has been proved very effective in predicting cloud characteristics compared with other cloud-cover schemes (Delworth et al., 2006; Hogan et al., 2001; Tiedtke, 1993).

The Numerical Weather Prediction Center (NWPC) of China Meteorological Administration (CMA) has been devoted to developing its new generation of global medium numerical weather forecast system since 2007, based on the Global/Regional Assimilation and Prediction System (GRAPES_GFS). Most of the physical parameterization schemes in GRAPES_GFS were transplanted from the Weather Research & Forecast model (WRF; Xu et al. 2008). Because of the simple coupling and the lack of interactions between main physical processes, the clouds were significantly underestimated in GRAPES_GFS with its previous diagnostic cloud-cover scheme, especially in tropical areas (Ma et al., 2016). Similar underestimation of global cloud cover was found in the NCAR CAM5 global climate model that also employs the diagnostic approach (Wang et al., 2015). Recently, we have applied a prognostic cloud-cover scheme to enhance the performance of cloud simulation in GRAPES_GFS utilizing Tiedtks's cloud technique (Tiedtke, 1993). This study is to describe the new explicit prognostic cloud-cover scheme and examine its simulation performance along with its impact on radiation against the previous diagnostic cloud-cover scheme in our forecast system.

This paper is organized as follows. Section 2 provides a brief description of GRAPES_GFS with its previous diagnostic and current prognostic cloud-cover schemes. Section 3 introduces the experimental setup used in this study. The simulation results using the new prognostic cloud-cover scheme are presented in section 4. A summary is provided in section 5.

2. Model Description and Cloud-Cover Schemes

2.1. GRAPES_GFS

GRAPES_GFS is a system that includes both atmospheric model and data assimilation component. The atmospheric model is a fully compressible nonhydrostatic model utilizing vector wind, potential

temperature, and exner pressure as independent variables. Based on the LAT-LON grid, it discretizes the spatial variables in the staggered Arakawa C grid and employs an off-centered two-time-level semiimplicit semi-Lagrangian scheme (2TL-SISIL) for time discretization. The height-based terrain-following coordinate with the Charney-Phillips variable staggering in the vertical direction is adopted in the GRAPES_GFS model. The data assimilation component uses three-dimensional variation data assimilation system (3DVar).

The physical parameterizations in the model mainly include RRTMG LW/SW radiation scheme (Morcrette et al., 2008; Pincus et al., 2003), Common Land Model (CoLM) scheme (Dai et al., 2003), MRF planetary boundary layer scheme (Hong & Pan, 1996), and New Simplified Arakawa-Schubert (NSAS) shallow and deep convection scheme (Arakawa & Schubert, 1974; Liu et al., 2015; Pan & Wu, 1995). For cloud processes, a large-scale cloud condensation scheme and a modified version of two-moment cloud microphysical scheme (Chen et al., 2007; Liu et al., 2003) were coupled into GRAPES_GFS. For the modified two-moment cloud microphysical scheme, it includes the calculation of mixing ratios of cloud water, raindrop, ice crystal, snow and graupel, and number concentrations of the four latter hydrometeors. At the same time, we applied an explicit prognostic cloud-cover scheme following Tiedtke's considerations (Tiedtke, 1993) to the system to replace the original Xu and Randall's diagnostic method (Xu & Randall, 1996). We next describe the two cloud-cover schemes.

2.2. Diagnostic Cloud-Cover Scheme

The original diagnostic cloud-cover scheme (hereafter DIAGCS) followed Xu and Randall's scheme in GRAPES_GFS (Xu & Randall, 1996). Cloud cover (C) is achieved as a function of relative humidity (RH), and large-scale grid-averaged condensate mixing ratio ($\bar{q}_\ell$). This scheme can be expressed as the following formulation:

$$C=\begin{cases} 1, & RH \geq 1 \\ RH^p\left[1-\exp\left(\dfrac{-\alpha_0 \bar{q}_\ell}{[(1-RH)q_{vs}]^\gamma}\right)\right], & RH < 1 \end{cases} \tag{1}$$

where γ, α_0, and p are nondimensional empirical coefficients and q_{vs} is the saturation mixing ratio. The determined γ, α_0, and p values from the Global Atmospheric Research Program's (GARP's) Atlantic Tropical Experiment (GATE) simulation are 0.49, 100, and 0.25, respectively. These parameters are used in the simulations of early version of GRAPES_GFS.

It can be seen from equation (1) that cloud cover will gradually approach its upper limit as condensation water content increases and that when $RH \geq 1$ in grid cell, a 100% cloud cover is reached.

2.3. Explicit Prognostic Cloud-Cover Scheme

The new explicit prognostic cloud-cover scheme (hereafter PROGCS) was explored in GRAPES_GFS based on Tiedtke's prognostic cloud scheme (ECMWF Documentation, 2012; Tiedtke, 1993). PROGCS directly link the generation and dissipation of cloud cover to large-scale horizontal and vertical transport, cumulus convection, and large-scale cloud condensation and evaporation processes. In this scheme, the prognostic equation of cloud cover is expressed as

$$\frac{\partial C}{\partial t}=A(C)+S(C)_{CV}+S(C)_{SC}-D(C) \tag{2}$$

where $\frac{\partial C}{\partial t}$ is the time change rate of cloud cover, $A(C)$ represents the change rate of cloud cover due to large-scale horizontal and vertical transport through the boundaries of the grid volume, $S(C)_{CV}$ and $S(C)_{SC}$ are the formation rate by cumulus convection and stratiform condensation processes, respectively, and $D(C)$ is the rate of decrease of cloud cover due to evaporation and precipitation. Actually, the change of cloud cover is also associated with the contribution from the boundary layer processes, which has been examined in our early studies (Jiang et al., 2015). The simulation in this study has turned off this influential factor from boundary layer processes.

Cloud-cover generations associated with NSAS cumulus convective processes are parameterized as condensates produced in the updrafts and detrained into the environmental air. The source term of cloud cover from NSAS is described as

$$S(C)_{CV}=(DR)_{up}+\frac{(MF)_{up}}{\rho}\frac{\partial C}{\partial z} \tag{3}$$

where ρ is the density of moist air (kg/m^3), $(DR)_{up}$ and $(MF)_{up}$ are the rate of relative mass detrainment (s^{-1}), and the net mass flux (kg/m^2/s) in the updrafts, respectively. The first term in equation (3) represents the relative detrainment rate of cloud cover from the NSAS convective updrafts and the second term is the vertical advection rate of cloud cover because of compensating subsidence in the environmental air. Note that the NSAS scheme has separated into deep and shallow convection processes, which correspond to term $S(C)_{CV\_deep}$ and $S(C)_{CV\_shallow}$, respectively. In the NSAS scheme, a threshold value (200 hPa) of the cloud thickness is adopted as the classification indicator between shallow convection and deep convection. For all convections, if the cloud thickness is greater than 200 hPa, deep convection processes are used; otherwise, shallow convection processes are used.

The parameterization of cloud-cover formations associated with stratiform clouds is based on the principle that condensation processes are determined by the rate at which the saturation specific humidity decreases due to the nonconvective processes such as large-scale lifting of moist air and radiative cooling. The rate of increase of cloud cover is calculated using the following formula:

$$S(C)_{SC}=\frac{-(1-C)^2}{2}\frac{1}{(q_{sat}-q_v)}\frac{dq_{sat}}{dt} \qquad \frac{dq_{sat}}{dt}<0 \tag{4}$$

where q_{sat} is saturation specific humidity (kg/kg) and q_v is grid-mean specific humidity (kg/kg). The constraint $S(C)_{SC}<\frac{(1-C)}{\Delta t}$ is imposed to ensure realistic value of C in equation (4) when values of q_v are close to saturation. In equation (4), the calculation of q_{sat} has considered the contributions from both the liquid and ice supersaturation. q_{sat} is defined as

$$q_{sat}=\alpha q_{sat(w)}+(1-\alpha)q_{sat(i)} \tag{5}$$

where $q_{sat(w)}$ and $q_{sat(i)}$ are the saturation specific humidities with respect to water and ice, respectively, and α is the fraction of water in the saturation specific humidity. For mixed-phase stratiform clouds, the fraction of ice in the saturation specific humidity is described as

$$\begin{cases} \alpha=0 & T\le T_{ice} \\ \alpha=\left(\frac{T-T_{ice}}{T_0-T_{ice}}\right)^2 & T_{ice}<T<T_0 \\ \alpha=1 & T>T_0 \end{cases} \tag{6}$$

where T_{ice} and T_0 represent the threshold temperatures between which a mixed phase is allowed to exist and are chosen as $T_{ice}=250.16$ K and $T_0=273.16$ K.

The dissipation of clouds is mainly caused by horizontal turbulent mixing of cloudy air with unsaturated environmental air, which is described as a diffusion process proportional to the saturation deficit of the air $CK(q_{sat}-q_v)$. At the same time, the larger the in-cloud water content, the more difficult or the lower the clouds can be dissipated. In other words, the dissipation of clouds should be also inversely proportional to in-cloud water content. Thus, similar as ECMWF, the expression for cloud fraction decrease rate associated with dissipation is

$$D(C)=\frac{CK(q_{sat}-q_v)}{q^{cld}} \tag{7}$$

where the diffusion coefficient $K=3\times10^{-6}$s^{-1} and q^{cld} is the specific cloud water/ice content. q^{cld} can be calculated by grid-mean specific cloud liquid water content q_l (kg/kg) and cloud cover C using

$$q^{cld}=q_l/C \tag{8}$$

Combined with equation (8), equation (7) becomes

$$D(C)=\frac{C^2K(q_{sat}-q_v)}{q_l} \tag{9}$$

3. Methodology

3.1. Experimental Setup

Two sets of global simulations were conducted in this study, one with DIAGCS and the other with PROGCS. Both simulations in this study are run at 0.25° × 0.25° horizontal resolution with 60 sigma vertical levels and a 300 s time step (DT), using the National Centers for Environmental Predication Final Operational Global Analysis (NCEP FNL; 1.0° × 1.0°) data as initial fields (Kalnay et al., 1996; available online at http://dss.ucar.edu/datasets/ds083.2/). The physical schemes used in the experiments have been presented in section 2.1.

Each set of simulation was carried out for 2 months, January and July 2013. For each simulation, the model started at 12UTC of every day and was integrated up to 120 h with 6-hourly interval outputs. We have averaged all 6-hourly outputs from 0000 through 1800 UTC to obtain daily mean data sets. Thus, model forecasts averaged over lead times of 12, 18, 24, and 30 h are termed as day-1 forecasts in this study. Longer lead times follow similarly. Day-3 forecasts have been used and analyzed in this study. The monthly mean is the averaged value of all daily mean data sets.

Additionally, two more specific cases were simulated starting at 12UTC on 1 July 2009 and 12 UTC on 1 June 2013 to investigate the impacts of PROGCS on radiation and diurnal cycle of cloud cover. The low, middle, high, and total cloud covers (LCC, MCC, HCC, and TCC) are calculated in GRAPES_GFS using a mixed cloud overlap assumption of maximum and random (Hogan & Illingworth, 2000; Mace & Benson-Troth, 2002). For clouds with adjacent layers, maximum cloud overlap assumption is used; and for clouds with nonadjacent layers, random cloud overlap assumption is used. In the model's sigma coordinates, the low, middle, high, and total clouds are defined as follows:

Low clouds: $p > 0.8p_{surf}$
Middle clouds: $0.8p_{surf} \leq p \leq 0.45p_{surf}$
High clouds: $p < 0.45p_{surf}$
Total clouds: $p_{top} < p < p_{surf}$

where p is the pressure, p_{surf}, and p_{top} are the surface pressure and the model top pressure, respectively.

3.2. Evaluation

To evaluate the simulation performance of PROGCS and its impacts on radiation process, four kinds of data sets are used in this study. The following several types of data sets were utilized to analyze the distributions of simulated cloud cover by PROGCS against DIAGCS on different spatial and temporal scales. One is the cloud-cover data sets from a surface site of the U.S. Department of Energy's Atmospheric Radiation Measurements (ARM) program (Stokes & Schwartz, 1994), the Southern Great site Plains (SGP) located at (36.6°N, 97.5°W). The second is the 6-hourly low level cloud cover from ERA-Interim data with 0.25° horizontal resolution (Naud & Booth, 2014; Dee et al., 2011). The third one is the monthly cloud cover from the Cloud and Earth's Radiant Energy System (CERES) SYN1deg cloud property retrievals based on Moderate Resolution Imaging Spectroradiometer (MODIS) radiance observations on Terra and Auqa with a spatial resolution of 1° × 1° (Minnis et al., 2008; Wielicki et al., 1996). While cloud cover from MODIS has their own uncertainties (Wang & Zhao, 2017), the uncertainties are not considered in this study. In addition, the outgoing longwave radiation (OLR) data at top of atmosphere (TOA) from CERES retrievals and the radiative heating rate from ECMWF Year of Tropical Convection (ECMWF-YOTC, Waliser et al., 2012) analysis data have been used to analyze the influences of cloud cover on the radiation processes. The model simulations with cloud-cover schemes of PROGCS and DIAGCS are linearly interpolated to meet the spatial resolution of observation and reanalysis data sets for bias calculation.

4. Results

In order to analyze the actual contributions from each source and sink terms to the cloud-cover simulations using the explicit prognostic cloud-cover scheme, the vertical distributions of zonal means of cloud fraction associated with deep convection and shallow convection detrainments and vertical advection, the large-scale stratiform cloud formation and cloud-cover evaporation are surveyed first. Second, two set experiments are simulated to test the forecast performance for cloud-cover vertical distributions at ARM SGP ground site and its diurnal variation at Peru marine stratocumulus region. Third, the global monthly mean

cloud covers from the two schemes are compared with CERES retrievals, respectively. Finally, the influences of cloud cover simulated via PROGCS on OLR at TOA and radiative heating rates are investigated.

4.1. Source and Sink Terms of Cloud Cover

Figure 1 shows the simulated zonal-mean cross sections and horizontal distributions of cloud-cover formation rate (CCFR) at 850 hPa from deep convection and shallow convection processes from 1 to 3 July 2013. The contributions of deep convection and shallow convection processes to CCFR are mainly distributed in the mid-low latitudes (60°S–60°N), especially in the tropical low latitude areas. However, there are evident differences in the vertical distributions for CCFR from different convection processes (Figures 1a and 1b). It can be seen that the CCFR from deep convection nearly distributed throughout the troposphere in tropical areas, which has a peak value more than 10%/DT from 950 to 150 hPa (Figure 1a). However, the maximum height with value of CCFR greater than 10%/DT only reaches 400 hPa in middle latitudes of Southern Hemisphere (SH), for the CCFR values in the middle latitudes of Northern Hemisphere (NH), they are almost less than 10%/DT. Similarly, there is a high value area in the region from 950 to 550 hPa along the storm track (50°S–30°S) in July 2013 (Figures 1a and 1c). These distribution characteristics are all related to the deep convection activities. Unlike deep convection, the shallow convection associated CCFR distributions with values greater than 10%/DT are located only below 700 hPa, but with a larger high value range. For regions with latitudes from 60°S to 30°N, the CCFR from shallow convection process is even higher with values up to 10%/DT or more (Figure 1b). Actually, the CCFR can be as high as 90%/DT in active marine stratocumulus regions such as off the west coast of Australia or Peru (Figure 1d). It is easy to draw the conclusion that shallow convection is a more important process for the cloud-cover contribution at low levels compared with deep convection.

The results of CCFR from total convection processes and large-scale stratiform condensation process, the cloud-cover evaporation rate (CCER) caused by turbulent mixing diffusion, and the actual cloud covers simulated by PROGCS are presented in Figure 2. As described in the above paragraph, the cloud-cover formation from total convection process mainly occurs in the areas of 60°S–60°N. The convection penetrates almost through the entire troposphere in the low latitudes, up to 100 hPa, while the highest height with CCFR greater than 1%/DT in the midlatitudes occurs near 400 hPa (Figure 2a). There is a high CCFR value zone with more than 20%/DT at the heights between 995 and 850 hPa, at which the largest amount can be up to 40%/DT or more. Figure 2b exhibits that the CCFR from stratiform condensation process has a wider

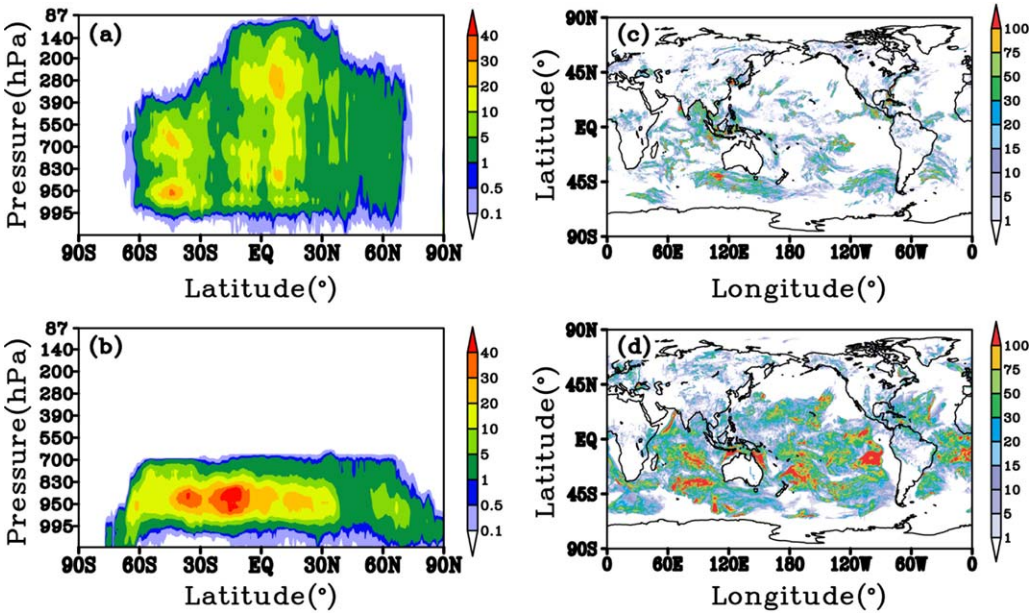

Figure 1. (left column) Zonal-mean cross sections and (right column) global distributions at 850 hPa of cloud-cover formation rate from (a, c) deep convection and (b, d) shallow convection processes averaged from 1 to 3 July 2013 (unit: %/DT).

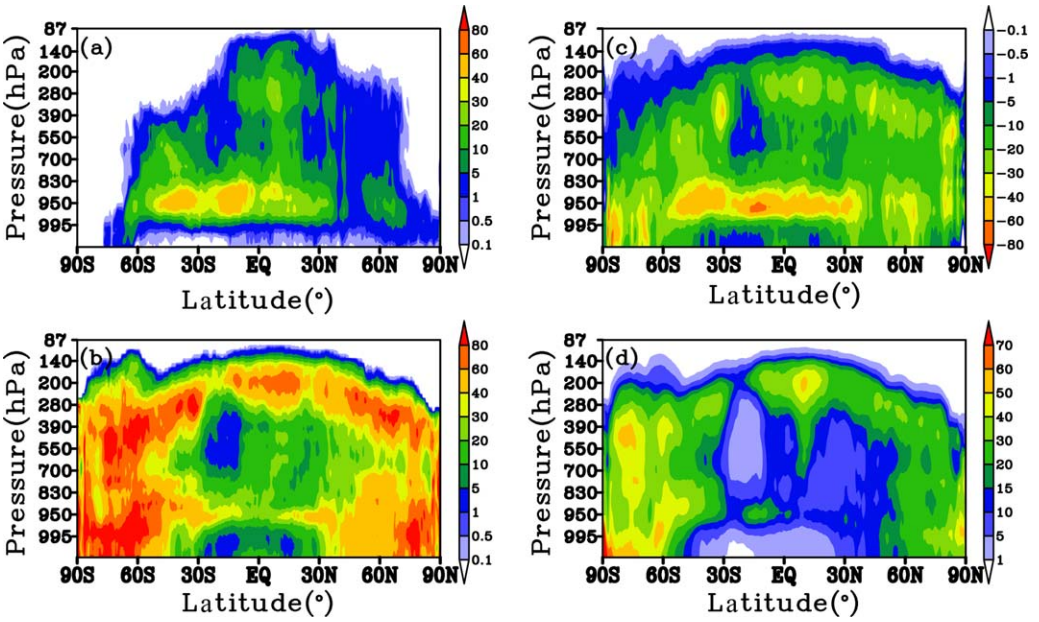

Figure 2. Zonal-mean cross sections of cloud cover (unit: %) and its formation and dissipation terms (unit: %/DT) averaged from 1 to 3 July 2013. (a) Formation rate by total cumulus convection, namely, from shallow convection and deep convection; (b) formation rate by stratiform condensation; (c) evaporation rate by turbulent mixing process; (d) actually simulated cloud cover.

range and higher values than that of convection process, which reveals stratiform condensation process as the main contributor to the cloud-cover formation. The high CCFR value zones in Figure 2b are mainly located in the middle and high latitudes (45°S–90°S and 45°N–90°N) and its height distributions can reach up to 250 hPa where most CCFR values are more than 30%/DT and even up to 80%/DT. In addition, there are two high value regions at heights near 950 hPa and at 300–100 hPa in low latitudes, while the CCFR values at the other regions are below 10%/DT. These distribution characteristics of CCFRs are closely related to the combination effect of large-scale stratiform condensation process and convection process. The spatial distributions of CCER shown in Figure 2c are very similar to those of CCFR from stratiform condensation process, except that there is a more clearly evaporating zone near 950 hPa in the middle and low latitudes (50°S–30°N). In general, the values of CCER are less than those of CCFR. The simulated cloud covers have a larger amount in the mid-high latitudes than those in tropical areas. In short summary, the CCFR in mid-high latitudes is dominated by stratiform condensation processes and is associated with the combined contributions of convection process and stratiform condensation process in low latitudes. However, cloud evaporation and convective precipitation are strong due to the intensive turbulence mixing and strong vertical motion in low latitudes, respectively, which cause the cloud cover in this area lower than that in mid-high latitudes.

4.2. Cloud-Cover Distributions and Diurnal Cycle

The ARM SGP site has a suite of active remote sensing instruments that provide vertical cloud structure information, which can be used to evaluate the simulated cloud cover. Figure 3 shows the 6-hourly vertical distributions of cloud cover from ARM retrievals and simulated via PROGCS and DIAGCS at the location of SGP site in January and July 2013. On a whole, PROGCS has an advantage over DIAGCS in the aspects of cloud occurrence frequency, vertical structure and magnitude of cloud cover compared with ARM observations. Specifically, the values of occurrence frequency from the ARM retrievals in January and July 2013 are 13.5% and 19.7%, respectively. The PROGCS significantly improved the frequency of cloud cover compared with DIAGCS: the cloud-cover values from DIAGCS run are 8.1% and 7.8% while those from the former can reach up to 11.4% and 19.9% during the two corresponding months in 2013. ARM retrievals illustrate clearly that there are two meteorological regimes passed through the SGP site from 8 to 16 January and from 23 to 30 January in 2013 (Figure 3a). Although the GRAPES_GFS runs with the two schemes both well captured the starting and ending time of the regimes, there are still clear differences in the distributions of cloud

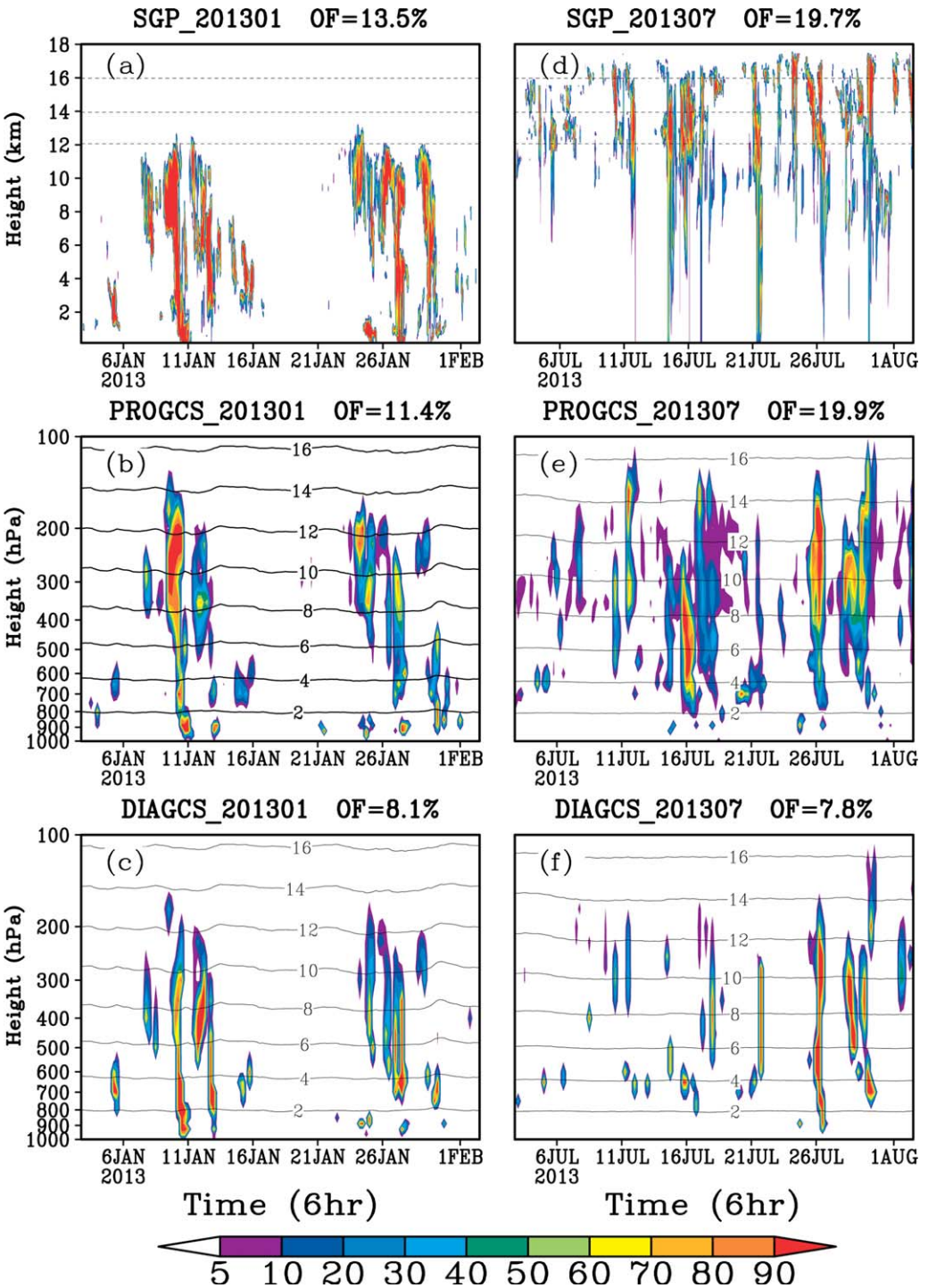

Figure 3. Six-hourly vertical distributions of cloud cover (a, d) from ARM observations, and simulated with (b, e) PROGCS and (c, f) DIAGCS over SGP site for (left column) January and (right column) July 2013 (unit: %). The shaded areas indicate the cloud cover greater than 5% and the contour lines represent the height (unit: km). The value at the top-right of each graph is the occurrence frequency of cloud cover.

cover (Figures 3a–3c). The vertical structures of cloud cover and their values above 4 km height from PROGCS run are more consistent with the observations compared with those from DIAGCS run during the two meteorological regimes. For instance, the maximum values of cloud cover simulated by PROGCS from 9 to 11 January 2013 occurred at the heights of 6–12 km, which are close to ARM retrievals, yet the

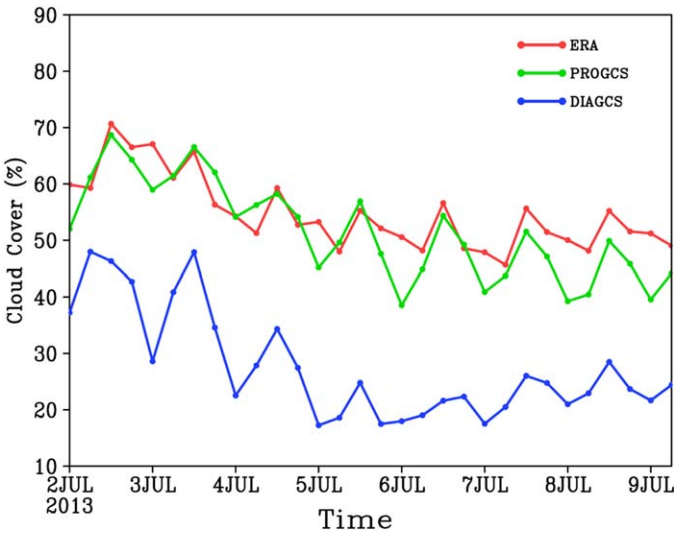

Figure 4. Six-hourly variation of averaged LCC from ERA (red line), simulated by PROGCS (green line) and DIAGCS (blue line) off the west coast of Peru (−30°S to −10°S, 80°W–110°W) during 2 June to 10 June 2013 (unit: %).

corresponding values and their duration simulated by DIAGCS are less and shorter than observations. Similar results can be found for the latter meteorological regime. However, the heights of cloud tops from PROGCS run are a little higher than those from ARM observations. It is evident that PROGCS was better at simulating the thickness, duration and vertical structures of cloud cover than DIAGCS during July 2013 (Figures 3d–3f), particularly for clouds above 4 km. Actually, PROGCS tends to produce deeper clouds than DIAGCS, which are up to near 16 km or even higher altitudes. Considering that most of the cloud top heights from ARM retrievals reach near or above 16 km, PROGCS seems perform more reliably. Note that PROGCS has overestimated the thin mid-high level clouds on days 1–15 July 2013. By contrast, DIAGCS run has apparently underestimated cloud cover: most of cloud tops are below 14 km and their durations are very short (Figure 3f).

In large-scale models, the amount of subtropical marine stratocumulus is usually underpredicted (Jakob, 1999). Because stratocumulus clouds can act as the result of those feedbacks that reduce the intensity of tropical convection, these biases have a significant influence on the (sub) tropical circulation (Ma et al., 1996; Miller, 1997). Therefore, the life cycle of stratocumulus cloud covers is evaluated using ERA data in this subsection. Figure 4 shows the 6-hourly variation of averaged LCC at Peru marine stratocumulus region. It is clear that the diurnal-cycle characteristics of LCC from ERA data are more similar to those simulated with PROGCS than to those simulated with DIAGCS. Although the DIAGCS runs also demonstrated the diurnal change signal, it seriously underestimated the LCC at marine stratocumulus region. By contrast, PROGCS performed well on predicting the amount of LCC: its maximum values show reasonable agreement with ERA data over days from 2 June to 7 June and its minimum values are consistent with ERA during the period from 2 June to 5 June. After 5 June, the low values of LCC simulated by PROGCS have a systematic negative bias of about −10%, which may be related to the suppressed shallow convection at night time.

4.3. Monthly Results

Figures 5 and 6 show the monthly mean distributions of TCC and their differences between model simulations and CERES for January and July 2013, respectively. In Figure 5, it can be seen that PROGCS has better ability to represent the distributions and amounts of TCC than DIAGCS in January and July 2013. Taking the simulation results of January 2013 as an example, the most significant difference between the two schemes is the simulation of TCC in low latitudes (30°S–30°N). Obviously, the TCCs in the Intertropical Convergence Zone (ITCZ) regions, the Warm Pool areas, and the main marine stratocumulus regions located off the west coast of Peru or California, have been reasonably simulated by PROGCS compared with CERES, while they were substantially underestimated by DIAGCS with biases up to −20% to −40%. In general, the distributions of higher TCC areas in the mid-high latitudes of SH (90°S–30°S) and NH (30°N–90°N) were well simulated by the two schemes. However, the TCCs along the storm track in SH were both underestimated, where PROGCS has less negative biases against DIAGCS. The differences in distribution characteristics of simulated TCC between PROGCS and DIAGCS are basically the same for July as for January. Though there are up to 10% overestimations over some ocean areas for PROGCS, the global mean bias of TCC has been dramatically reduced by using the PROGCS scheme, which has been reduced from −25.9% to −5.06% in January and from −27.0% to −2.83% in July 2013 (Figure 6).

The performance of simulated monthly averaged cloud cover at different altitudes (LCC, MCC and HCC) has also been shown in Figure 7. CERES retrievals indicate that LCC has a low value of ∼20% in low latitudes, but increases toward midlatitudes and high latitudes with the maximum value of 80% in January and July 2013 (Figures 7a and 7d). PROGCS and DIAGCS simulations have both reproduced the same distributions as CERES, except for high-latitude regions of winter hemisphere. However, there are systematic negative biases for the two simulations compared to the CERES retrievals. It is encouraging that PROGCS has evidently decreased the biases compared with DIAGCS, especially in low latitude tropical areas. For example, the

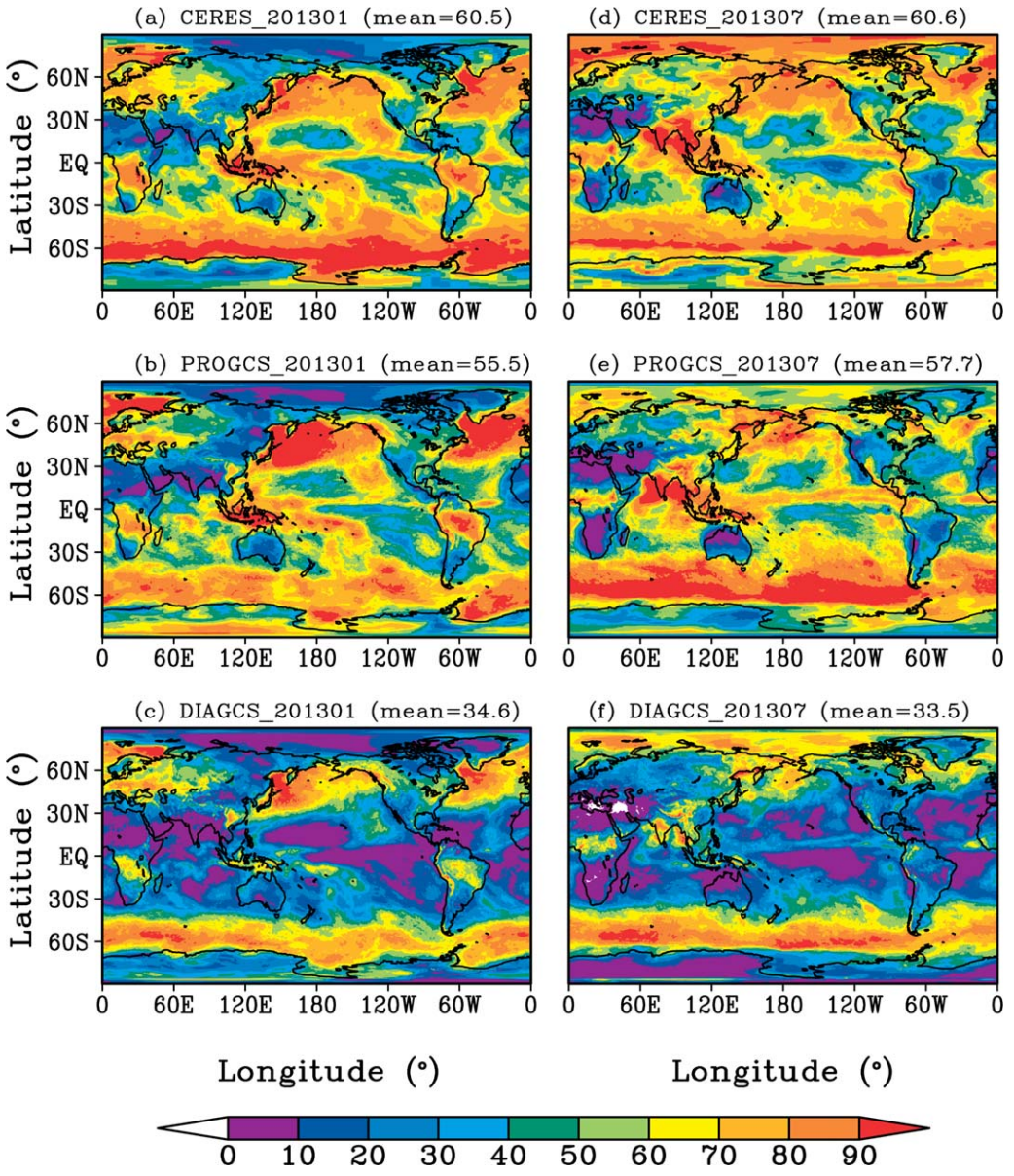

Figure 5. Monthly mean total cloud cover (a, b) observed by CERES satellite and simulated by (b, e) PROGCS and (c, f) DIAGCS for (left column) January 2013 and (right column) July 2013 (unit: %).

averaged negative bias decreases from −18.2% to −7.8% at 40°S–30°N region during the period of January 2013. As mentioned in section 4.1, one possible reason to this improvement is that the cloud-cover formation term from shallow convection processes has been considered in PROGCS. The LCCs with large biases in the high latitudes of winter hemisphere (60°N–90°N in January and 90°S–60°S in July) has been also slightly reduced by using PROGCS. Of course, there is a positive bias over the Antarctic continent in January for PROGCS (Figures 6a and 7a). Figure 7 also shows that PROGCS has an advantage over DIAGCS with less negative biases in simulating MCCs in the high-latitude regions. By contrast, for regions other than high latitudes, such as areas of 60°S–60°N, the PROGCS performs even worse than the DIAGCS by showing larger positive biases in MCCs compared to CERES observations. For instance, there is a maximum bias of near 20% for MCCs simulated by PROGCS at 50°S in January (Figure 7b). Figures 7c and 7f reveal that the simulations of HCCs have been improved too by using PROGCS, which are more consistent with the CERES retrievals than those simulated using DIAGCS almost in all latitudes. Actually, DIAGCS seriously underestimated the amounts of HCCs. For example, the maximum biases in HCCs for simulating with DIAGCS occur at

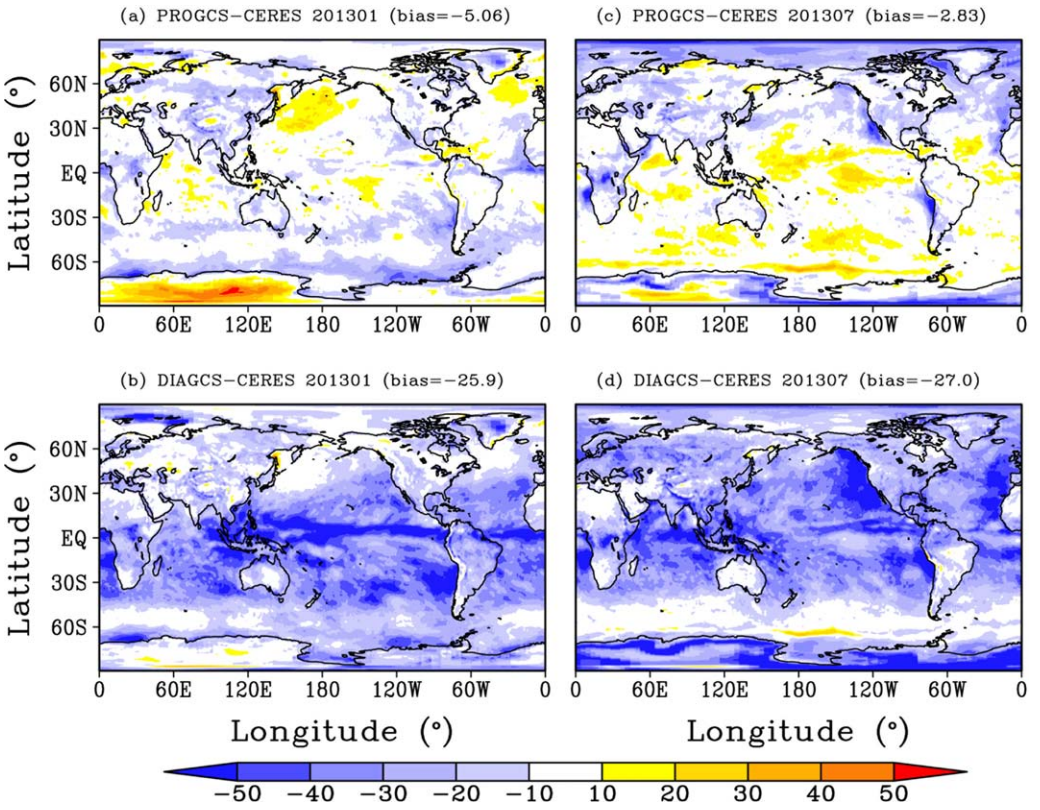

Figure 6. Monthly mean differences of total cloud cover between CERES observation and model simulation with (a, c) PROGCS and (b, d) DIAGCS for (left column) January and (right column) July 2013 (unit: %). Biases are computed from the model minus CERES observation.

tropical areas (20°S–20°N) with values up to near −30% in January, while the biases are only −8.9% for simulations with PROGCS.

Overall, PROGCS has significantly improved the model performance in simulating LCCs and HCCs, causing much less negative biases. Nevertheless, it should be noted that PROGCS induces an even larger positive biases for MCCs simulations against DIAGCS in 60°S–60°N latitude region.

4.4. Radiation Flux and Heating Rate

The impacts of the improved cloud covers determined by PROGCS on OLR at TOA and radiative heating rate were investigated here. Figure 8 shows the monthly mean differences of OLR at TOA between the CERES retrievals and the simulations by the GRAPES model with schemes of PROGCS and DIAGCS. It demonstrates that the systematic overestimation of OLR has been significantly reduced by using the simulations of cloud cover with the scheme of PROGCS instead of DIAGCS. Compared to simulations with DIAGCS, the global mean bias of OLR for simulations with PROGCS is reduced from 10.7 to 4.38 W m^{-2} in January and from 9.98 to 3.92 W m^{-2} in July 2013, respectively. There is a significant reduction of OLR simulation bias in regions over tropical ocean, storm track of SH and middle latitudes of NH. For example, the biases of OLR at Warm Pool region (5°S–20°N, 100°E–160°E) are large with values up to 50 W m^{-2} for simulations with DIAGCS but are much smaller with values generally below 30 W m^{-2} for simulations with PROGCS. For the whole tropical belt (20°S–20°N), the mean OLR amount of CERES is 254.8 W m^{-2} in January 2013, and the values simulated by the GRAPES model with schemes of PROGCS and DIAGCS are 269.4 and 261.0 W m^{-2}, respectively. We can see that the mean bias has decreased 8.4 W m^{-2} over the whole tropical belt by using PROGCS. In addition, the areas where the largest reduction of OLR biases occurs are consistent with the regions where the maximum change of TCCs bias are located, as shown in Figures 6 and 8. Thus, the reduction of OLR bias should be associated with the improvement of simulated cloud cover via PROGCS. Actually, we have also found better simulation performance in shortwave radiation at both TOA and surface by using

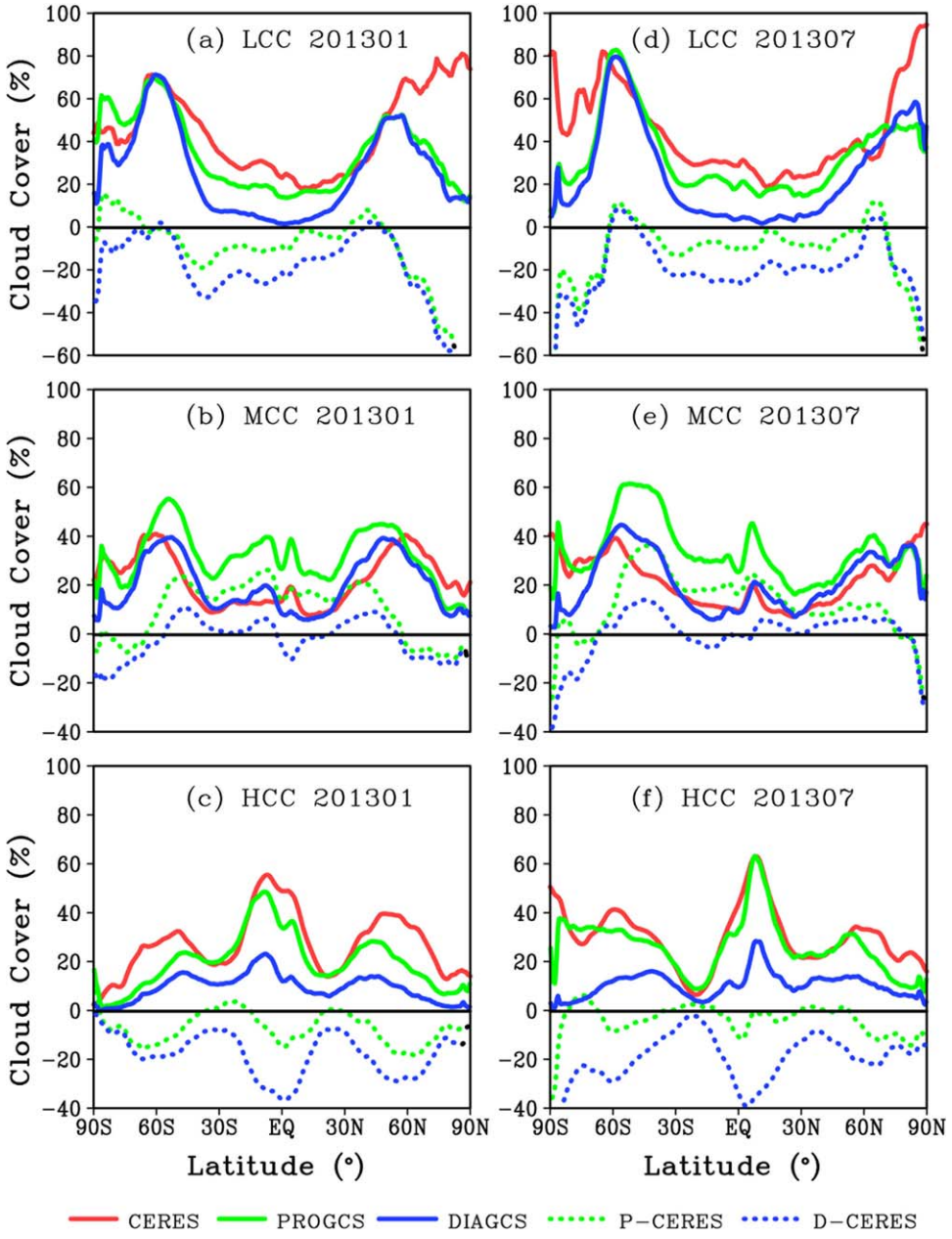

Figure 7. Monthly zonal mean of (a, d) LCC, (b, e) MCC, and (c, f) HCC from CERES observation (red line) and model simulation with PROGCS (green solid line) and DIAGCS (blue solid line) and their biases (PROGCS: green dotted line; DIAGCS: blue dotted line) against CERES for (left column) January and (right column) July 2013 (unit: %).

PROGCS compared to DIAGCS. For example, the downwelling shortwave radiation has significant improvement at surface in the tropical region by using PROGCS. The details about the shortwave radiation simulations are not shown here.

Profiles of spatial and temporal averaged temperature tendencies associated with the radiation process in YOTC and GRAPES_GFS simulations are shown in Figure 9. It appears that total radiative temperature cooling tendency is 1.0–1.5 K/d between 950 and 250 hPa and less than 0.5 K/d at bottom and upper model levels (Figure 9a). The two runs with PROGCS and DIAGCS have both captured the basic features of the profiles same as YOTC, yet the bias of temperature tendency is less for the simulations with PROGCS than that with DIAGCS. There is a systematic negative bias with values of −0.1 to −0.5 K/d for DIAGCS at heights from 850

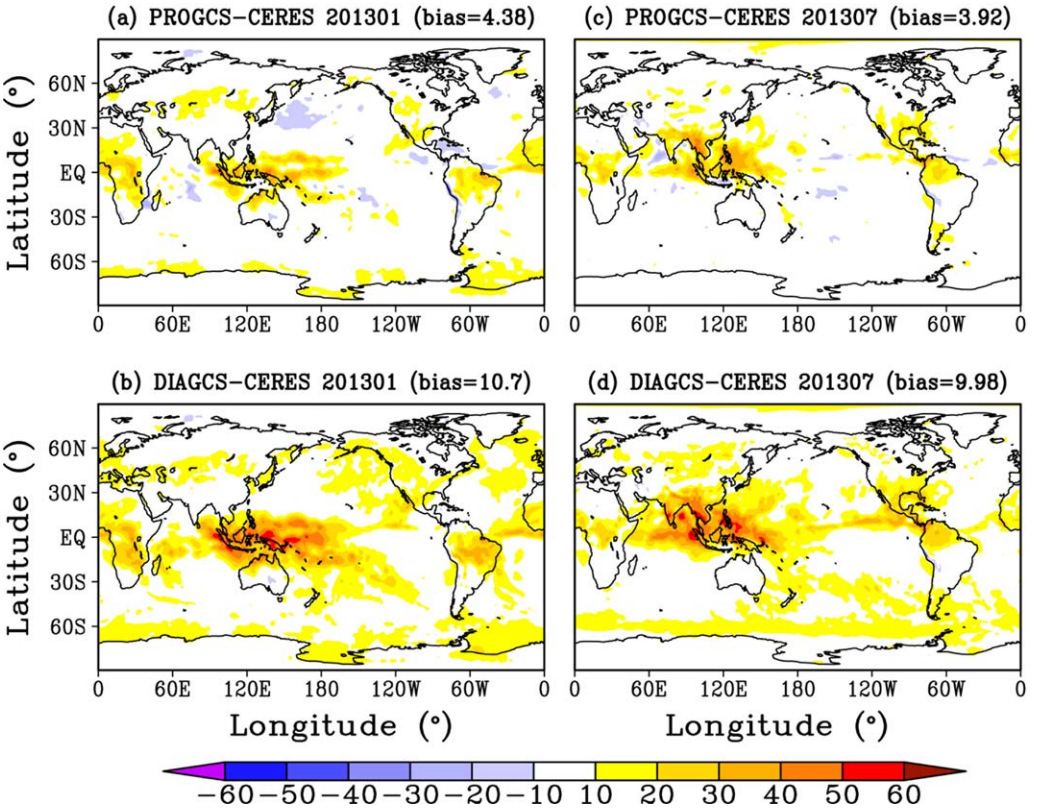

Figure 8. Same as Figure 6, but for the monthly mean biases of OLR at TOA simulated with PROGCS and DIAGCS as compared to CERES retrievals (unit: W m^{-2}).

to 750 hPa. As shown in section 4.3 (Figure 7), PROGCS has significantly improved the simulations of LCCs and HCCs, which leads to smaller biases of temperature tendency from PROGCS runs against DIAGCS runs at heights below 850 hPa and above 400 hPa. In contrast, the positive biases in temperature tendency

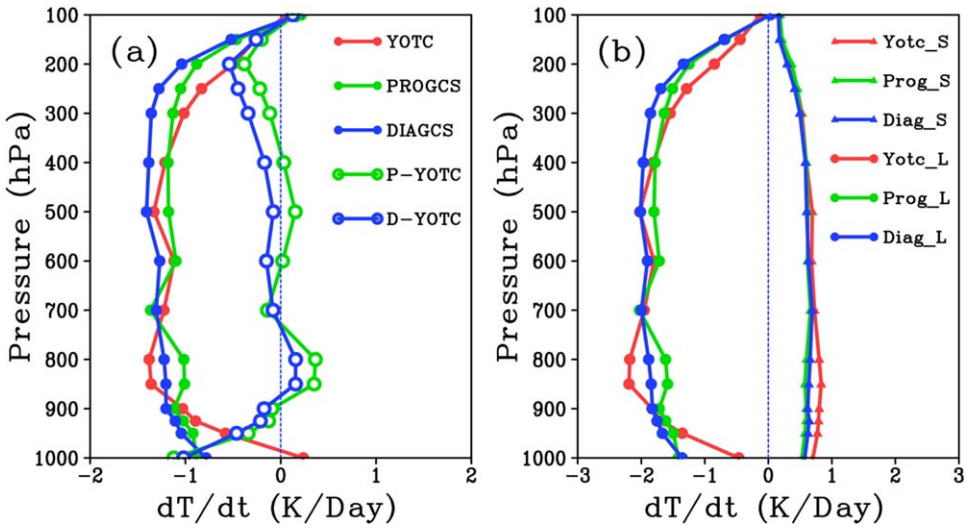

Figure 9. Vertical profiles of global mean radiative heating rate (unit: K d^{-1}) from (red line) YOTC and model simulations with (green line) PROGCS and (blue line) DIAGCS during 00UTC, 2 July and 00UTC, 3 July 2009. In Figure 9a, it shows (closed circle) the total (LW + SW) radiative heating rate and (open circle) its differences compared with YOTC and it plots the heating rates from (closed circle) LW and (closed triangle) SW in Figure 9b, respectively.

produced by PROGCS run at 800 and 500 hPa levels are probably related to the overestimation of MCCs. The temperature tendencies caused by SW simulations with the two schemes are quite consistent, and their biases compared to YOTC are very small with a maximum value of only 0.2 K/d at 850 hPa. As shown in Figure 9b, we still can see slight improvements at both upper and lower levels for the simulations with PROGCS (Figure 9b). Moreover, the profiles of temperature tendency associated with LW for the two simulations are very similar to those of total radiative heating rate. These imply that the modification of LW is likely one of the main reasons to the simulation improvement of total radiative heating rate in GRAPES_GFS. At high levels (400–100 hPa), OLR biases have been reduced as a result of more HCCs from PROGCS simulations compared with DIAGCS, which give rise to less radiative cooling from LW and present a more consistent profile with YOTC (Figures 8 and 9).

5. Summary and Conclusions

It is a long-lasting problem of how to represent cloud cover in large-scale global models. To enhance the capability of predicting cloud cover, an explicit prognostic cloud-cover scheme (PROGCS) based on the work by Tiedtke (1993) has been implemented into NWPC of CMA in recent years. By comparing the simulations of the global operational forecasting system (GRAPES_GFS) with original diagnostic (DIAGCS) and current PROGCS cloud-cover schemes, we analyze the performance of the new PROGCS scheme. The contributions of each source and sink terms in the PROGCS are investigated quantitatively. The simulation performance of cloud covers from the two schemes and their impacts on OLR and radiative heating rates are evaluated with satellite retrievals, reanalysis data and in site observations. The results can be summarized as follows:

1. The impact of deep convection processes on cloud-cover formation rate (CCFR) is clear over most of the troposphere in tropical areas, yet the CCFR from shallow convection mainly occur below 700 hPa. The total CCFRs at low latitudes arise from the combinations of convection and stratiform condensation processes, while they are primarily caused by large-scale stratiform condensation process in mid and high latitudes. Among all the source terms, large-scale stratiform condensation process is the most important contributor to the CCFR on the global scale, and its high values (up to more than 30%/DT) mainly occur at mid-high latitudes and at upper levels of tropical areas. The evaporation of clouds caused by turbulent mixing is too strong to lead cloud cover with low values at low latitudes.
2. The vertical structures and magnitudes of cloud cover simulated by PROGCS are generally more consistent with observations at ARM SGP site than those simulated with DIAGCS. Based on the ERA reanalysis data, the simulations with PROGCS have well reproduced the diurnal cycle of marine stratocumulus with less biases in low level cloud cover and stronger signals of diurnal cycle off the west coast of Peru compared with the simulations with DIAGCS.
3. The PROGCS has greater advantage than the DIAGCS in simulating TCCs, LCCs, and HCCs. The systematic negative biases of TCCs simulated with DIAGCS has been significantly reduced by using PROGCS from −25.9% to −5.0% in January 2013 and from −27.0 to −2.83% in July 2013, respectively. Similarly, the biases of LCCs and HCCs have been reduced as well. Differently, it should be noted that there is an evident overestimation for MCCs by using PROGCS at low-mid latitudes (60°S–60°N), where the average positive bias is up to 14% in January and 18% in July 2013, respectively.
4. Associated with the improvement of cloud-cover simulations, the OLR biases simulated with PROGCS against CERES retrievals have been notably reduced compared to that with DIAGCS both in January and July 2013, especially in tropical areas and storm track regions. Moreover, the profiles of total temperature tendencies simulated with PROGCS are more reasonable than those simulated with DIAGCS by comparing with YOTC at levels below 850 hPa and above 400 hPa due to better model simulation performance to LCC and HCC as shown in Figure 7. It seems that the modification of cloud cover has a more remarkable impact on temperature tendency associated with LW radiation than that associated with SW radiation. In other words, the differences of temperature tendency profiles associated with LW are close to those associated with total radiation (LW plus SW).

PROGCS is a more physically based scheme compared with the original scheme of DIAGCS because PROGCS is connected with the cloud formation and dissipation processes. GRAPES_GFS with PROGCS has significant

improvements in the simulations of cloud cover and radiation, while there is an overestimation for MCCs in low-middle latitudes. In future, the simulation of MCCs could also be improved by limiting the value of CCFR from convection processes, such as the approach proposed by Park et al. (2014).

Acknowledgments
This paper is jointly supported by the Ministry of Science and Technology of China (2017YFC1501403 and 2017YFC1501406), the National Natural Science Foundation of China (NSFC) (grants 41575143, 41105067, and 41375107), Special Fund for Meteorology Scientific Research in the Public Interest (grants GYHY201506018 and GYHY201406005), the State Key Laboratory of Earth Surface Processes and Resource Ecology (2017-ZY-02), and the Fundamental Research Funds for the Central Universities. Coauthor Y.W. appreciates the funding support provided by US National Science Foundation (NSF, award 1700727). Coauthor J.H.J. acknowledges the support by the Jet Propulsion Laboratory, California Institute of Technology, sponsored by NASA. The data used in this study can be downloaded via ftp: nwpc.nmc.cn (user: pub, pswd: verygood) and are also available by request to Zhanshan Ma through mazs@cma.gov.cn.

References

Akihiko, S., Masao, K., Sam, F. I., & Hong, S. Y. (2008). Comparison of four cloud schemes in simulating the seasonal mean field forced by the observed sea surface temperature. *Monthly Weather Review*, *136*, 2557–2575.

Arakawa, A., & Schubert, W. H. (1974). Interaction of a cumulus cloud ensemble with the large-scale environment, Part I. *Journal of the Atmospheric Sciences*, *31*, 674–701.

Cantrell, W., & Heymsfield, A. (2005). Production of ice in tropospheric clouds: A review. *Bulletin of the American Meteorological Society*, *86*, 795–807. https://doi.org/10.1175/BAMS-86-6-795

Chen, X. M., Liu, Q. J., & Zhang, J. C. (2007). A numerical simulation study on microphysical structure and cloud seeding in cloud system of QiLian Mountain Region [in Chinese]. *Meteorological Monthly*, *33*(7), 33–43.

Cotton, W. R., & Anthes, R. A. (1989). *Storm and cloud dynamics*. San Diego, CA: Academic.

Dai, F. S., Yu, R. C., Zhang, X. H., & Yu, Y. Q. (2004). A statistical low-level cloud scheme and its tentative application in a general circulation model (in Chinese). *Acta Meteorological Sinica*, *62*(4), 385–394.

Dai, Y. J., Zeng, X. B., Dickinson, R. E., Baker, I., Bonan, G. B., Bosilovich, M. G., et al. (2003). The Common Land Model. *Bulletin of the American Meteorological Society*, *84*(8), 1013–1023.

Dee, D. P., Uppala, S. M., Simmons, A. J., Berrisford, P., Poli, P., Kobayashi, S., et al. (2011). The ERA-Interim reanalysis: Configuration and performance of the data assimilation system. *Quarterly Journal of the Royal Meteorological Society*, *137*, 553–597.

Delworth, T. L., Broccoli, A. J., Rosati, A., Stouffer, R. J., Balaji, V., Beesley, J. A., et al. (2006). GFDL's CM2 global coupled climate models. Part I: Formulation and simulation characteristics. *Journal of Climate*, *19*, 643–674.

Dowling, D. R., & Radke, L. F. (1990). A summary of the physical properties of cirrus clouds. *Journal of Applied Meteorology*, *29*, 970–978.

ECMWF Documentation. (2012). *IFS documentation-Cy37r2 operational implementation 18 May 2011, Part IV: Physical processes* (pp. 91–106).

Hogan, R. J., Jakob, C., & Illingworth, A. J. (2001). Comparison of ECMWF winter-season cloud fraction with radar-derived valuses. *Journal of Applied Meteorology*, *40*, 513–525.

Hogan, R. J., & Illingworth, A. J. (2000). Deriving cloud overlap statistics from radar. *Quarterly Journal of the Royal Meteorological Society*, *126A*, 2903–2909.

Hong, S. Y., & Pan, H. L. (1996). Nonlocal boundary layer vertical diffusion in a medium-range forecast model. *Monthly Weather Review*, *124*, 2322–2339.

Huang, D., Campos, E., & Liu, Y. (2014). Statistical characteristics of cloud variability: 1. Retrieved cloud liquid water path at three ARM sites. *Journal of Geophysical Research: Atmospheres*, *119*, 10813–10828. https://doi.org/10.1002/2014JD022001

IPCC. (2013). Climate change 2013: The physical science basis. In T. F. Stocker et al. (Eds.), *Contribution of Working Group I to the Fifth Assessment Report of the Intergovernmental Panel on Climate Change* (1535 pp.). Cambridge, UK: Cambridge University Press. https://doi.org/10.1017/CBO9781107415324

Jakob, C. (1999). Cloud cover in the ECMWF reanalysis. *Journal of Climate*, *12*, 947–959.

Jiang, J. H., Su, H., Zhai, C., Perun, V. S., Del Genio, A., Nazarenko, L. S., et al. (2012). Evaluation of cloud and water vapor simulations in CMIP5 climate models using NASA "A-Train" satellite observations. *Journal of Geophysical Research*, *117*, D14105. https://doi.org/10.1029/2011JD017237

Jiang, X. F., Liu, Q. J., & Ma, Z. S. (2015). Influences of shallow convective process and boundary-layer clouds on cloud forecast in GRAPES global model [in Chinese]. *Meteorological Monthly*, *41*(8), 921–931.

Kalnay, E., Kanamitsu, M., Kistler, R., Collins, W., Deaven, D., Gandin, L., et al. (1996). The NCEP/NCAR 40-year reanalysis project. *Bulletin of the American Meteorological Society*, *77*, 437–471.

Klein, S., & Jakob, C. (1999). Validation and sensitivities of frontal clouds simulated by the ECMWF model. *Monthly Weather Review*, *127*, 2514–2531.

Liou, K. N. (1992). *Radiation and cloud processes in the atmosphere*. New York, NY: Oxford University Press.

Liou, K.-N., & Ou, S. C. (1989). The role of cloud microphysical processes in climate: An assessment from a one-dimensional perspective. *Journal of Geophysical Research*, *94*, 8599–8607. https://doi.org/10.1029/JD094iD06p08599

Liu, K., Chen, Q., & Sun, J. (2015). Modification of cumulus convection and planetary boundary layer schemes in the GRAPES global model. *Journal of Meteorological Research*, *29*(5), 806–822.

Liu, Q. J., Hu, Z. J., & Zhou, X. J. (2003). Explicit cloud scheme of HLAFS and simulation of heavy rainfall and clouds, Part I: Explicit cloud scheme [in Chinese]. *Journal of Applied Meteorological Science*, *14*, 60–67.

Ma, C.-C., Mechoso, C. R., Robertson, A. W., & Arakawa, A. (1996). Peruvian stratus clouds and the tropical Pacific circulation: A coupled ocean-atmosphere GCM study. *Journal of Climate*, *9*, 1635–1646.

Ma, Z. S., Liu, Q. J., & Qin, Y. Y. (2016). Validation and evaluation of cloud and precipitation forecast performance by different moist physical processes schemes in GRPAES_GFS model. *Plateau Meteorology*, *35*(4), 989–1003. https://doi.org/10.7522/j.issn.1000-0534.2015.00069

Mace, G. G., & Benson-Troth, S. (2002). Cloud-layer overlap characteristics derived from long-term cloud radar data. *Journal of Climate*, *15*, 2505–2515.

Miller, R. L. (1997). Tropical thermostats and low cloud cover. *Journal of Climate*, *10*, 409–440.

Minnis, P., Trepte, Q. Z., Sunmack, S., Chen, Y., Doelling, D. R., Young, D. F., et al. (2008). Cloud detection in nonpolar regions for CERES using TRMM VIRS and Terra and Aqua MODIS data. *IEEE Transactions on Geoscience and Remote Sensing*, *46*, 3857–3884. https://doi.org/10.1109/TGRS.2008.2001351

Morcrette, J.-J., Barker, H. W., Cole, J. N. S., Iacono, M. J., & Pincus, R. (2008). Impact of a new radiation package, McRad, in the ECMWF Integrated Forecast System. *Monthly Weather Review*, *136*, 4773–4798.

Naud, C. M., & Booth, J. F. (2014). Evaluation of ERA-Interim and MERRA cloudiness in the Southern Ocean. *Journal of Climate*, *27*, 2109–2124.

Pan, H.-L., & Wu, W. S. (1995). *Implementing a mass flux convective parameterization package for the NMC medium-range forecast model* (NMC Office Note 409, pp. 1–40). Washington, DC: NMC.

Park, R.-S., Chae, J.-H., & Hong, S.-Y. (2016). A revised prognostic cloud fraction scheme in a global forecasting system. *Monthly Weather Review*, *144*, 1219–1229. https://doi.org/10.1175/MWR-D-15-0273.1

Park, S., Bretherton, C., & Rasch, P. (2014). Integrating cloud processes in the community atmosphere model, version 5. *Journal of Climate*, *27*, 6821–6856.

Pincus, R., Barker, H. W., & Morcrette, J.-J. (2003). A fast, flexible, approximate technique for computing radiative transfer in inhomogeneous cloud fields. *Journal of Geophysical Research*, *108*(D13), 4376. https://doi.org/10.1029/2002JD003322

Randall, D. A. (1989). Cloud parameterization for climate modeling: Status and prospects. *Atmospheric Research*, *23*, 345–361.

Randall, D. A., Coakley, J. A., Jr., Lenschow, D. H., Fairall, C. W., & Kropfli, R. A. (1984). Outlook for research on subtropical marine stratification clouds. *Bulletin of the American Meteorological Society*, *65*(12), 1290–1301.

Randall, D. A., Harshvardhan, Dazlich, D. A., & Corsetti, T. G. (1989). Interactions among radiation, convection, and large-scale dynamics in a general circulation model. *Journal of the Atmospheric Sciences*, *46*, 1943–1970.

Rybka, H., & Tost, H. (2014). Uncertainties in future climate predictions due to convection parameterizations. *Atmospheric Chemistry and Physics*, *14*, 5561–5576. https://doi.org/10.5194/acp-14-5561-2014

Slingo, J. M. (1987). The development and verification of a cloud predication scheme for the ECMWF model. *Quarterly Journal of the Royal Meteorological Society*, *113*(477), 899–927.

Soden, B. J., & Held, I. M. (2006). An assessment of climate feedbacks in Coupled Ocean-Atmosphere Models. *Journal of Climate*, *19*, 3354–3360.

Stocker, T. F., Qin, D., Plattner, G.-K., Tignor, M., Allen, S. K., Boschung, J., et al. (2013). *Climate change 2013: The physical science basis* (1535 pp.). Cambridge, UK: Cambridge University Press. Retrieved from www.climatechange2013.org/images/report/WG1AR5_ALL_FINAL.pdf

Stokes, G. M., & Schwartz, S. E. (1994). The Atmospheric Radiation Measurement (ARM) program: Programmatic background and design of the cloud and radiation test bed. *Bulletin of the American Meteorological Society*, *75*, 1201–1221.

Sundqvist, H., Berge, E., & Kristjansson, J. E. (1989). Condensation and cloud parameterization studies with a mesoscale numerical weather predication model. *Monthly Weather Review*, *117*, 1641–1657.

Teixeira, J. (2001). Cloud fraction and relative humidity in a prognostic cloud fraction scheme. *Monthly Weather Review*, *129*, 1750–1753. https://doi.org/10.1175/1520-0493(2001)129<1750:CFARHI>2.0.CO;2

Tiedtke, M. (1993). Representation of clouds in large-scale models. *Monthly Weather Review*, *121*, 3040–3061. https://doi.org/10.1175/1520-0493(1993)121<3040:ROCILS>2.0.CO;2

Tompkins, A. M. (2002). A prognostic parameterization for the subgrid-scale variability of water vapor and clouds in large-scale models and its use to diagnose cloud cover. *Journal of the Atmospheric Sciences*, *59*, 1917–1942.

Tompkins, A. M. (2005). *Moist processes lecture notes series: The parameterization of cloud cover* (ECMWF Tech. Memo. 1–23). Retrieved from http://www.ecmwf.int/publications

Wang, S. (1996). Defining marine boundary layer clouds with a prognostic scheme. *Monthly Weather Review*, *124*, 1817–1833.

Wang, Y., Fan, J., Zhang, R., Leung, R., & Franklin, C. (2013). Improving bulk microphysics parameterizations in simulations of aerosol effects. *Journal of Geophysical Research: Atmospheres*, *118*, 5361–5379. https://doi.org/10.1002/jgrd.50432

Wang, Y., Jiang, J. H., & Su, H. (2015). Atmospheric responses to the redistribution of anthropogenic aerosols. *Journal of Geophysical Research: Atmospheres*, *120*, 9625–9641. https://doi.org/10.1002/2015JD023665

Wang, Y., & Zhao, C. (2017). Can MODIS cloud fraction fully represent the diurnal and seasonal variations at DOE ARM SGP and Manus sites? *Journal of Geophysical Research: Atmospheres*, *122*, 329–343. https://doi.org/10.1002/2016JD025954

Waliser, D. E., Moncrieff, M. W., Burridge, D., Fink, A. H., Gochis, D., Goswami, B. N., et al. (2012). The "year" of tropical convection (May 2008–April 2010): Climate variability and weather highlights. *Bulletin of the American Meteorological Society*, *93*, 1189–1218.

Wetzel, M. A., & Bates, G. T. (1995). Comparison of simulated cloud cover with satellite observations over the western United States. *Journal of Climate*, *8*, 296–314. https://doi.org/10.1175/1520-0442(1995)008<0296:COSCCW>2.0.CO;2

Wielicki, B. A., Barkstrom, B. R., Harrison, E. F., Lee, R. B., III, Smith, G. L., & Cooper, J. E. (1996). Clouds and the Earth's Radiant Energy System (CERES): An earth observing system experiment. *Bulletin of the American Meteorological Society*, *77*, 853–868.

Wilson, D. R., Bushell, A. C., Kerr-Munslow, A. M., Price, J. D., & Morcrette, C. J. (2008a). PC2: A prognostic cloud fraction and condensation scheme, I: Scheme description. *Quarterly Journal of the Royal Meteorological Society*, *134*, 2093–2107. https://doi.org/10.1002/qj.333

Wilson, D. R., Bushell, A. C., Kerr-Munslow, A. M., Price, J. D., Morcrette, C. J., & Bodas-Salcedo, A. (2008b). PC2: A prognostic cloud fraction and condensation scheme. II: Climate model simulations. *Quarterly Journal of the Royal Meteorological Society*, *134*, 2109–2125. https://doi.org/10.1002/qj.332

Xu, K.-M., & Randall, D. A. (1996). A semiempirical cloudiness parameterization for use in climate model. *Journal of the Atmospheric Sciences*, *53*, 3084–3102. https://doi.org/10.1175/1520-0469(1996)053<3084:ASCPFU>2.0.CO;2

Xu, K. Q., Chen, D. H., Xue, J. S., Sun, J., Shen, X. S., Shen, Y. F., et al. (2008). Optimization experiment and program structure design of GRAPES physical processes. *Chinese Science Bulletin*, *53*(20), 2428–2434.